Contrib Mineral Petrol (2003) 145: 1–14
DOI 10.1007/s00410-003-0440-7

ORIGINAL PAPER

Garrett B. Hazelton · Gary Axen · Oscar Lovera

Argon retention properties of silicate glasses and implications for $^{40}Ar/^{39}Ar$ age and noble gas diffusion studies

Received: 16 December 2001 / Accepted: 18 November 2002 / Published online: 13 February 2003

Abstract Sized aggregates of glasses (47–84 wt% SiO_2) were fused from igneous-derived cohesive fault rock and igneous rock, and step-heated from ~400 to > 1,200 °C to obtain their ^{39}Ar diffusion properties (average $E = 33{,}400$ cal mol^{-1}; $D_o = 4.63\times10^{-3}$ cm^2 s^{-1}). At $T < \sim$1,000 °C, glasses containing $< \sim$69 wt% SiO_2 and abundant network-forming cations (Ca, Fe, Mg) reveal moderate to strong non-linear increases in D and E, reflecting structural modifications as the solid transitions to melt. Extrapolation of these Arrhenius properties down to typical geologic T-t conditions could result in a 1.5 $\log_{10}$ unit underestimation in the diffusion rate of Ar in similar materials. Numerical simulations based upon the diffusion results caution that some common geologic glasses will likely yield $^{40}Ar/^{39}Ar$ cooling ages rather than formation ages. However, if cooling rates are sufficiently high, ambient temperatures are sufficiently low (e.g., < 65–175 °C), and coarse particles (e.g., radius (r) > ~1 mm) are analyzed, glasses with compositions similar to ours may preserve their formation ages.

Introduction

The investigation of thermally-activated volume diffusion of Ar in geologic materials has been an ongoing effort for several decades (McDougall and Harrison 1999). These experimental results form the basis for the $^{40}Ar/^{39}Ar$ method of thermochronology that is widely applied to minerals and, to a lesser extent, glasses. Although the ability of the $^{40}Ar/^{39}Ar$ method to interpret age and thermal history data from rocks depends on many factors, knowing the Ar transport properties of any dated material (crystalline or non-crystalline) is critical. Glass is commonly present in igneous rocks, impact-related rocks (e.g., tektites), and shear-heated fault rocks (i.e., pseudotachylyte). This paper describes the experimentally-derived Ar diffusion properties of some fused silicate glasses and discusses the implications of numerical cooling simulations, which incorporate these diffusion parameters, for interpreting $^{40}Ar/^{39}Ar$ ages from glasses of similar compositions. Particular emphasis has been placed upon understanding $^{40}Ar/^{39}Ar$ ages from glasses produced by shear heating (e.g., pseudotachylyte) along buried faults, although our results are easily applied to simpler cooling scenarios (e.g., rapidly cooled volcanic rocks or tektites).

Pseudotachylyte, a type of fault rock generally formed in the upper 15 km of the crust during seismic slip along faults and within ductile shear zones, is argued to be the product of ultracataclasis, frictional fusion, or a combination of these processes (e.g., Sibson 1975, 1977; Wenk 1978; Magloughlin and Spray 1992; Spray 1995). The rock is also associated with impact structures (e.g., Shand 1916; Reimold 1995; Thompson et al. 1998). Although pseudotachylyte is known to occur in many polymineralic rock types, it most commonly occurs in granitoid rocks. The definition of pseudotachylyte is based on macro- and micro-scale characteristics that include occurrence as typically dark, mostly aphanitic veins that appear to be intrusive in nature, presence of included mineral fragments and wall-rock clasts, sharp vein margins, and close association with faults and shear zones (Sibson 1975; Magloughlin and Spray 1992). The matrix component of these veins is typically microcrystalline (r < 100 μm) to cryptocrystalline minerals. In addition, veins may include glass, neoblastic minerals recrystallized from glass, vesicles, spherulites, and microlites (Sibson 1975; Magloughlin and Spray 1992). When the presence of one

Electronic Supplementary Material is available if you access this article at http://dx.doi.org/10.1007/s00410-003-0440-7. On that page (frame on the left side), a link takes you directly to the supplementary material.

G.B. Hazelton · G. Axen (✉) · O. Lovera
Department of Earth and Space Sciences,
University of California Los Angeles,
595 Charles Young Dr. E, Los Angeles, CA 90095, USA
E-mail: gaxen@ess.ucla.edu
Tel.: +1-310-8253880

Editorial responsibility: K. Hodges

or more of these textural features is observed in pseudotachylyte veins along a fault, slip-induced frictional fusion of ultracomminuted material along the fault is typically inferred (Magloughlin and Spray 1992). However, note that the absence or presence of glass alone is not a prerequisite in classifying or identifying a rock as pseudotachylyte; its presence only helps demonstrate a melt origin of the rock.

In general, any glass that is present in the matrix portion of a given pseudotachylyte vein is not readily separable from the non-glassy component, is not easily distinguished from adjacent fine-grained crystalline material without the use of a transmission electron microscope (TEM), is difficult to avoid when analyzing a pseudotachylyte using standard $^{40}Ar/^{39}Ar$ analytical techniques, and probably has diffusion properties that are quite different than the non-glassy components. Given that pseudotachylyte can form and endure in active, probably fluid-rich, tectonic environments, it is not surprising that glass, if ever present in a given vein, is usually only locally preserved and in very few instances does it constitute the major component of a pseudotachylyte vein (e.g., Scott and Drever 1953; Sinha-Roy 1981; Lin 1994). Nonetheless, it does occur, making it is necessary to consider how the diffusion properties of Ar in glass may affect the bulk $^{40}Ar/^{39}Ar$ age of a highly heterogeneous material like pseudotachylyte, especially if one wishes to interpret the geologic significance of the age (e.g., cooling versus generation).

In an attempt to detail the enigmatic slip histories of faults and shear zones and date impact events, a growing number of investigations have focused on $^{40}Ar/^{39}Ar$ dating of fault rocks (e.g., pseudotachylyte) either by furnace step-heating (e.g., Reimold et al. 1990; Trieloff et al. 1994; Wenk et al. 2000), or laser probe analysis (e.g., Karson et al. 1998; Kelley et al. 1994; Spray et al. 1995; Thompson et al. 1998). Samples analyzed in these investigations apparently contain little if any glass, although rigorous TEM analysis to document the presence of glass is not always specified. Due to the highly heterogeneous nature of pseudotachylyte matrix at all scales, and the desire to avoid visible wall rock and mineral clasts that may retain an argon component inherited from the host protolith, the laser probe has become the preferred tool for $^{40}Ar/^{39}Ar$ analysis of pseudotachylyte because it offers precise spatial analysis (typical beam width between 10 and 100 μm) of the micro- to cryptocrystalline matrix that surrounds larger clasts. Scanning electron microscope (SEM) mapping of the sample matrix is critical in accurately targeting desired materials while avoiding others. Even so, because inter- and intrasample K content and radiogenic ^{40}Ar yield can vary, it is commonly necessary to raster shallow pits over an ~100-μm wide region in order to collect a sufficient volume of gas. However, if a sample has not also been characterized with a TEM, the presence of glass cannot be precluded within the area of laser analysis and Ar may be extracted from a mixture of minerals and glass, each of which has unique diffusion properties and may have experienced a different history of Ar loss or retention. $^{40}Ar/^{39}Ar$ dating of pseudotachylyte vein formation is based on the assumptions that the material analyzed was outgassed upon formation of the vein and subsequently closed to diffusive Ar loss shortly after vein formation. Thus, understanding how Ar retention varies as a function of ambient temperature, cooling rate, material composition, and grain size, is fundamental to testing these assumptions.

In this study we measure the Ar diffusion properties of a pure sanidine glass and glasses prepared from a basalt rock and three natural samples of comminuted fault rock (e.g., pseudotachylyte), and compare these data with those from previous silicate glass Ar diffusion experiments (Carroll 1991; Carroll and Stolper 1991; Roselieb et al. 1995). Unlike these earlier studies, which used an electron microprobe to measure Ar concentration profiles across a sectioned sample, we use a bulk sample, furnace step-heating approach to measure the diffusion of nucleogenic ^{39}Ar. The furnace method, like alternative analytical techniques (e.g., laser, electron probe), assumes that the diffusion mechanisms and measured diffusion profiles mimic those in nature (McDougall and Harrison 1999). This application of furnace-derived diffusion data to natural argon loss is not without contention (cf. Parsons et al. 1999; Lovera et al. 2002). The debate focuses on potential intracrystalline microstructural changes that may affect the subsolidus distribution and retention properties of Ar in anhydrous minerals such as K-feldspar, and whether these changes can be reproduced in vacuo under the experimental temperature–time conditions. However, such concerns have rarely, if ever, been raised in regards to structurally simple, end-member materials such as silicate glasses, which have been routinely step-heated for decades (McDougall and Harrison 1999). On this basis, the furnace step-heating approach is used to measure the Ar diffusion properties of the silicate glasses. Although our step-heating approach differs from most previous glass diffusion studies, our diffusion data are consistent with other published results and arguably better suited for interpreting $^{40}Ar/^{39}Ar$ bulk step-heating age measurements. Thermal history calculations performed using our glass diffusion data demonstrate that, under most geologic conditions in which glass-bearing fault pseudotachylyte is likely to form, quantitative retention of K-derived Ar in the glass will likely begin long after the faulting (i.e., glass formation) event and fault exhumation (i.e., glass cooling) ages will result. This has implications for the interpretation of $^{40}Ar/^{39}Ar$ age results obtained from any glass-bearing pseudotachylyte or other glasses (e.g., volcanic, tektite) that have undergone slow-cooling or experienced reheating.

Sample selection and experimental methods

Five distinct glasses are analyzed in this investigation. The sanidine glass (S1; Table 1) is a pure, synthetic glass

Table 1 Major oxide compositions of the sanidine (S) pseudotachylyte-derived (P) and alkali basalt-derived (AB) glasses

	S1	P1	P4	P5	AB[a]
SiO_2	64.75	84.26	60.95	69.61	46.77
MgO		0.22	2.96	1.63	9.92
Na_2O	0.67	0.74	2.82	3.34	2.80
Al_2O_3	18.03	9.06	17.01	16.96	13.87
FeO[b]	0.02[c]	1.46	6.48	8.57	12.31
MnO		0.02	0.03	0.03	0.15
K_2O	16.52	3.13	4.29	2.46	0.82
CaO		0.35	3.22	3.37	10.04
TiO_2		0.32	0.89	1.20	0.11
Cr_2O_3		0.03	0.02	0.13	2.15
Sum	99.39	99.59	98.67	98.38	98.86
ΣMelt time (h)		67.25[d]	66.4[e]	168.80[f]	~24

[a]Alkali basalt, Hualalai, Hawaii (cf. sample no. 20; Yoder and Tilley 1962)
[b]Total Fe reported as FeO unless otherwise noted
[c]Reported as Fe_2O_3 (White et al. 1989)
[d]Initial pre-melt mass 1.47 g
[e]Initial pre-melt mass 1.38 g
[f]Initial pre-melt mass ~1.0 g; time does reflect the actual time required tofully melt the material

(end-member $KAlSi_3O_8$ composition) obtained from Corning Glass (see also White et al. 1989). It was analyzed so that diffusion results yielded by our experimental approach could be compared with previous Ar diffusion data from equivalent material (Carroll 1991). The other glasses (P1, P4, P5, and AB; Table 1) were prepared by fusing, respectively, three natural samples of fine-grained, cohesive fault rock (i.e., pseudotachylyte) and an alkali basalt. The primary focus of this investigation is the diffusion behavior of Ar in the pseudotachylyte-derived glasses.

The goal of the P-glass production process is to produce a set of glasses that are compositionally similar to natural glasses that could occur in veins of fault pseudotachylyte and are derived from granitoid protoliths. To accomplish this, we extracted the micro- to cryptocrystalline matrix from three samples of granitoid-hosted, cohesive fault rock that were collected along outcrop-scale detachment faults in the Whipple Mountains, California (e.g., Davis and Anderson 1991), and melted each at 1,400 °C and 1 atm.

The low-silica (47 wt% SiO_2) AB-glass is derived from a powdered sample of alkali basalt rock from Hualalai, Hawaii, and serves as a compositional end member to compare and contrast with the more silicic P-glasses (Table 1). Such low-silica glasses are not expected in a glassy pseudotachylyte derived from a granitoid protolith, but could occur in a glassy pseudotachylyte derived from a mafic rock. The AB-glass was prepared in the same manner as the P-glasses. A detailed description and additional chemical analysis of the parent basalt rock can be found in Yoder and Tilley (their sample no. 20; 1962).

Representative samples of the prepared glasses were examined using the electron microprobe, SEM, and secondary electron backscatter imaging to assess composition and homogeneity. Crushing and sorting provided four size fractions for each of the three P-glass samples; two size fractions for the AB-glass. These 14 samples were irradiated with fast neutrons to produce ^{39}Ar, which was then measured during furnace step-heating to determine the bulk Ar diffusion properties of each sample. Details of these procedures are discussed below.

Fault rock sample selection

The P-glass production process is not designed to mimic the natural, complex process of pseudotachylyte glass formation, but to produce glasses that are compositionally similar to natural pseudotachylyte glasses. In as much as we are trying to evaluate by proxy the bulk diffusion properties of natural fault rock glasses, materials at least two to three generations removed from the original granitoid parent rocks, we felt it best to prepare our glasses from materials that span a range of immediate precursor (i.e., ultracomminuted host rock) compositions. The distribution of minerals across the width of a typical vein of fault rock is usually inhomogeneous, and is one of the many factors that can effect the final composition of any glass. While small-scale chemical variations within a single pseudotachylyte vein certainly exist, analyzing glasses from a single vein may have revealed few significant differences in the bulk Ar retention properties of those materials. To avoid this possibility, we chose to sample multiple veins, each derived from granitoid host rocks, and evaluate the effects of broad chemical heterogeneities that exist between them. Models outlining the mechanisms of pseudotachylyte formation (e.g., Spray 1995; Ray 1999; Tsutsumi 1999) suggest that during cataclasis (i.e., fault slip), the smallest particles are most susceptible to melting (other factors such as composition, water content, etc. being equal). By inference, if the faults from which our rock samples are collected were to slip, the fine-grained matrix material we extracted to make our glasses would arguably be most likely to melt.

On this basis, fine-grained matrix material, taken from three spatially-unrelated veins of cohesive fault rock, provided the starting materials for our pseudotachylyte-derived glasses. All three veins of fault rock were chosen solely because they are fine-grained and derived from granitoid (granodiorite to granite) protoliths (interested readers can refer to; Anderson and Cullers 1990, for chemical analyses of representative granitoid basement rocks in the Whipple Mountains) like many pseudotachylyte veins are. The fault rocks are dark in color, aphanitic, and contain included clasts of rock and mineral fragments. The fault rock veins occur along widely separated faults, have sharp, chilled vein margins, and display evidence of intrusion (see also Hazelton et al. 1998a, 1998b, 1999). Optical petrography indicates that all phases are crystalline (either primary mineral and rock fragments or minerals crystallized after

glass), X-ray diffraction (XRD) analysis indicates glass is not detectable at the 5% level, and a TEM analysis was not performed. We believe these rocks are altered/recrystallized pseudotachylytes. Electron microprobe, SEM, and XRD characterization of the fault rock matrix prior to melting allowed us to identify three samples with significant alkali feldspar contents. The high alkali feldspar contents guaranteed that the resulting glasses had adequate K_2O for ^{39}Ar production during irradiation, thereby ensuring that sufficient volumes of gas could be collected at each temperature step.

Glass preparation

For each of the three P-glass samples, fault rock vein matrix was segregated from mineral and rock clasts larger than ~0.2 mm, crushed in a clean alumina mortar, and transferred to a Pt–Au (95:5) crucible prior to fusion. The crucible surface had been pretreated with molten Fe-rich basalt to prevent Fe loss from the sample, then cleaned. Each crushed sample was loaded into the prepared crucible, heated for ~1 h at 1,100 °C in a muffle furnace, then immediately placed into a 1-atm Zircar furnace set at 1,400 °C. Heating occurred under a constant flow of N_2 gas to control potential changes in the oxidation state of Fe. After melting, the sample was drop-quenched in deionized water to limit crystal growth. Solidification occurred within a few seconds. The glass was extracted from the crucible, crushed, and examined under a 15× microscope to determine the degree of vesiculation and melting. All P-glass samples required multiple fusion cycles to produce crystal- and typically bubble-free glass; the AB-glass did not. Prior to remelting, glasses were repowdered in the previously used mortar. Total melt times are listed in Table 1. For the P-glasses, quartz, and to a lesser extent feldspar, were always the last minerals to melt. This is likely due to melting conditions (dry, low pressure) and the fact that the largest (ca. > 50 μm diameter) fragments (typically quartz and feldspar) were, on average, one to two orders of magnitude larger than all other minerals present after the initial crushing. Other minerals, along with the smaller quartz and feldspar fragments, typically melted during the first heating cycle. Between samples, the mortar was cleaned with SiO_2 power to remove surface contaminants, and the crucible was bathed overnight in hydrofluoric acid and resaturated with Fe-rich basalt.

Each final P-glass sample was crushed and particles sized into 55–70 (200–270 mesh), 130 (100–120 mesh), 350 (40–50 mesh), and 700 μm (20–30 mesh) diameter splits by sieving (Table 2). Two size fractions were produced for the basalt glass: 155 (80–100 mesh) and 350 μm (40–50 mesh) diameter grains. Approximately 25 mg of glass fragments were hand-selected from each of the 12 P-glass splits; ~30 mg from the two AB-glass splits. In most instances, the fragments selected were equant to sub-equant and lacked thin, feathered edges so as to most closely approximate a model diffusion geometry. At high magnifications, the surfaces of these grains are somewhat irregular due to conchoidal fracturing, but the fundamental geometry of each grain is best described as an edge-worn cube (1:1:1) or prism (~1.3:1:0.5). Optical analysis prior to step-heating indicated that grains were free of internal fractures, which could affect the diffusion results.

Compositional analysis

The degree of homogeneity of each P- and AB-glass sample was determined by backscattered electron imaging coupled with energy dispersive chemical analysis using a LEO-1430VP SEM. Multiple fragments (~1–3 mm diameter) of each glass sample were mounted in epoxy resin, polished, and carbon-coated prior to analysis. Element distribution maps show that all major elements are well mixed within each glass and that melting was ≥99% complete during the preparation process. Glasses usually lack post-quench neocrysts, but micron-size phases (typically restitic quartz or feldspar, or crucible-derived Pt) persist at the < 2% level in the P-glasses. Any fragments of glass containing restitic starting material were discarded. Internal fractures were not observed in any of the glass fragments, and vesicles were only notable in the most siliceous sample (P1, Table 1).

Table 2 Average diffusion parameters of sanidine (S) and pseudotachylyte-derived (P) glasses

Sample no. (effective radius)	^{39}Ar[a] (%)	E (cal mol^{-1})	$\log_{10}D_o/r_o^2$ (s^{-1})	$\log D_o$ (cm^2 s^{-1})
S1 (1,740 μm)	14.1 (16)	26,300 ± 300	−1.08 ± 0.09	−2.6 ± 0.09
P1-230 (30 μm)	97 (14)	26,100 ± 300	0.71 ± 0.08	−4.4 ± 0.22
P1-100 (65 μm)	99 (26)	26,900 ± 200	0.06 ± 0.20	−4.3 ± 0.16
P1-40 (175 μm)	94 (28)	29,400 ± 500	−0.26 ± 0.09	−3.8 ± 0.16
P1-20 (350 μm)	49 (28)	24,700 ± 100	−1.41 ± 0.03	−4.3 ± 0.05
P4-200 (35 μm)	93 (11)	37,200 ± 900	2.45 ± 0.19	−2.5 ± 0.12
P4–100(65 μm)	86 (14)	38,500 ± 800	2.27 ± 0.19	−2.1 ± 0.19
P4-40 (175 μm)	59 (14)	30,400 ± 900	−0.26 ± 0.22	−1.8 ± 0.22
P4-20 (350 μm)	48 (16)	36,900 ± 700	0.74 ± 0.15	−2.2 ± 0.14
P5-230 (27.5 μm)	98 (12)	36,600 ± 700	2.56 ± 0.16	−2.5 ± 0.14
P5-100 (65 μm)	87 (17)	36,600 ± 700	1.87 ± 0.17	−2.5 ± 0.19
P5-40 (175 μm)	49 (14)	38,600 ± 900	1.75 ± 0.19	−2.0 ± 0.28
P5-20 (350 μm)	26 (11)	36,200 ± 600	0.49 ± 0.12	−2.4 ± 0.12

[a]Cumulative %^{39}Ar release used in regression (number of steps used *in parentheses*; see also Figs. 1 and 2)

Major element composition data was obtained for the P- and AB-glasses and unresorbed precursor phases (e.g., quartz) by wavelength dispersive analysis using a JEOL JXA8200 electron microprobe. Analysis regions were identified using backscattered electron imaging. Element analysis was performed using a 15-keV accelerating potential, a 15-nA beam current, and 20-s count times. Glasses were analyzed with a 2-μm beam. Beam spot test results show a negligible drop in the counting signal from K over a 45-s interval. A 2-μm beam was also used to analyze the rare crystalline phases (e.g., SiO_2, metal oxides). Major oxide totals are given in Table 1.

^{39}Ar extraction and measurement

Irradiation procedures

Sized glass aggregates were packaged in Cu or Al foil, sealed in an evacuated quartz tube, and irradiated for 45 h in L67 position of the Ford Reactor, University of Michigan, to produce ^{39}Ar from ^{39}K. Neutron fluence was monitored with Fish Canyon sanidine (27.8 ± 0.3 Ma) flux monitors.

Furnace step-heating procedures

The step-heating procedures employed are modeled after those described in Lovera et al. (1997). Temperature within the double-vacuum resistance furnace was calibrated just prior to the experiments by monitoring the melting temperature of pure Zn, Al, and Cu. Samples were baked at ~200 °C prior to analysis to remove atmospheric surface contaminants. Step-heating was performed between ~300–1,650 °C. Flux monitor and ^{39}Ar step-heating data are given in the Supplementary Electronic Material. Although diffusion measurements are generally ignored beyond the temperature at which the material melts (T_m), higher temperature steps were analyzed to ensure thorough degassing of each sample because recovery of all ^{39}Ar within the sample is required to calculate accurate Ar diffusivities. Furnace pump-out times were minimized (~20 s) and temperature was maintained during pump-out. These procedures limit ^{39}Ar loss during successive heating steps to negligible quantities and avoid potential temperature control degradation and sample fracturing that thermal cycling could produce. After purification with a SAES ST-101 alloy getter pump, the ^{39}Ar was analyzed with a VG1200S noble gas mass spectrometer (Lovera et al. 1997).

Results and discussion

Comparison of bulk step-heating and depth-profiling diffusion experiments

The way in which our bulk step-heating experiments measure the diffusion properties of glasses significantly differs from the most common method used in previous studies. The latter employ electron microprobe depth-profiling of silicate glasses that had been isothermally heated in an Ar atmosphere, and diffusivities were calculated from measured variations in Ar concentration with distance from an experimental diffusion boundary (Carroll 1990, 1991; Carroll and Stolper 1991; Roselieb et al. 1992, 1995). In these investigations, depth profiles are only measured over a distance of up to 300 μm from the surface of the 4-mm wide sample, at 10–15-μm intervals. It is assumed that the measured length scales reflect all possible intra- and intersample variations for glasses of that composition. Although diffusion length scales are explicitly measured using this method, bulk properties that are equally important and more relevant to ^{40}Ar/^{39}Ar step-heating studies are not revealed. Conversely, the step-heating approach, when applied to anhydrous materials that are stable over the range of experimental investigation, can interrogate the diffusion properties of the entire volume of material by reproducing the natural diffusion mechanism (McDougall and Harrison 1999). While r is usually only estimated, this is not a concern for any thermal history modeling study provided that experimentally determined diffusion properties adequately mimic those that operate in nature (McDougall and Harrison 1999).

To illustrate how we interpret our step-heating results in terms of diffusion parameters, we first analyze data obtained from a single 50-mg fragment of sanidine glass (S1) and then compare the results (Table 2) with those from previous depth-profiling experiments performed with equivalent material (orthoclase; Carroll 1991). The analyzed fragment of S1 had the shape of an edge-worn cube. To estimate the diffusive length scale for this particle, we calculated the radius of a sphere of equivalent mass and density ($r = 0.176$ cm). Note that use of a rectangular or cubic geometry would not have significantly changed the results (see below and McDougall and Harrison 1999).

Sanidine glass (S1) diffusivities (D/r^2 in sec^{-1}) were calculated from the step-heating ^{39}Ar release data as outlined in Appendix A of Lovera et al. (1997). Successive isothermal measurements performed below 800 °C confirm the internal reproducibility of individual measurements under these conditions. Plots of diffusivity as a function of inverse temperature are presented in Fig. 1a for different assumed diffusion geometries. The difference between the calculated diffusion coefficients for the different geometries slightly decreases with increasing temperature, with the average difference between spherical and infinite slab geometry generally equal to one $\log_{10}$ unit at a given temperature. Note that the difference between rectangular and spherical results is minimal, and that a cubic geometry would have yielded similar results. In plotting the results on Fig. 1a, we normalized our measured D/r^2 values to $r = 1$ cm to facilitate comparison with previous diffusion measurements of Ar in glass. For a spherical diffusion geometry, the calculated diffusivities for S1 differ by less than a log

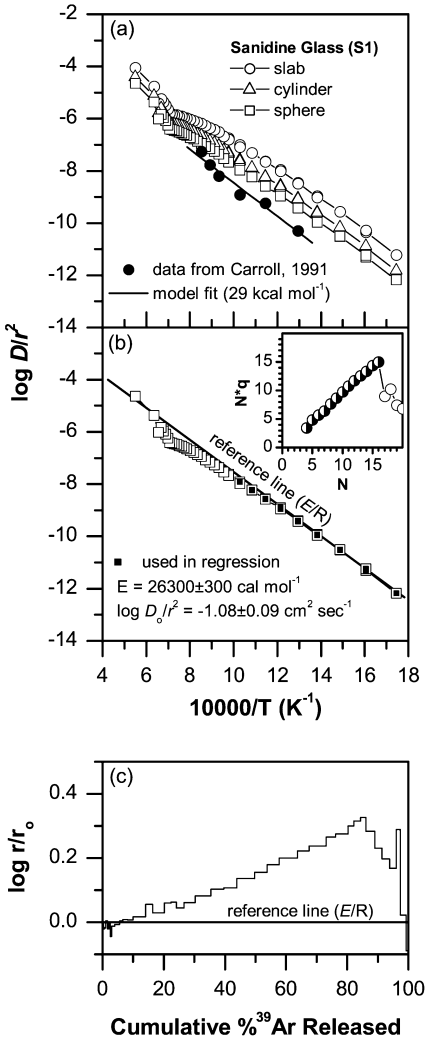

Fig. 1a–c Arrhenius diagrams and log r/r_o plot for Ar diffusion in sanidine glass. **a** Effect of diffusion geometry upon calculated diffusivities for S1 (this study). Note that all data are normalized to $r = 1$ cm. Results show that a spherical geometry most closely approximates the results of (Carroll 1991). **b** Methodology for regressing Arrhenius parameters determined from step-heating results. *Inset* shows statistical basis for selecting data points in regression where N is the number of steps beginning with the initial step and q is the goodness of fit (see Lovera et al. 1997). **c** Increase in the effective diffusion length scale (r) normalized by that obtained in **b** above (E/R; see text). Net observed increase of ~35% is not critical as additional data points could have been added to the regression without significantly affecting the reference line results

unit from, and at high temperature converge with, those reported by Carroll (1991), who represented his glasses with semi-infinite media geometry. The fact that our spherical geometry data closely mimic the older results indicates that the furnace step-heating method is appropriately interrogating the diffusion properties of S1.

It is difficult to unambiguously point to the factor(s) that may be causing the minor differences between the previous (Carroll 1991) and new (S1) results, in part because the older data are more scattered (Fig. 1). For example, the minor difference could be one of comparing different geometries (i.e., semi-infinite media versus spherical). Alternatively, our glass fragments, which are irregularly shaped, are modeled assuming an ideal, spherical geometry. Due to the irregular shape, through the low-temperature portion of the S1 data array, diffusivities may be higher than those expected from a perfect sphere because the initial Ar is extracted more easily from small corners and edges along the outer surface of the fragments. These corners and edges have a smaller r than the ideal r of the whole fragment. This effect is minimized at higher temperatures. The irregular, non-ideal surface topography caused by corner and edge effects is imparted during sample preparation (i.e., fracturing) and is unavoidable. We refer to this non-ideal surface geometry as shape anisotropy. Far from being detrimental, we argue that the rough surface geometry of our grains more closely approximates the non-ideal shape of a natural fragment of glass from a rock than does that of the semi-infinite geometry. On the basis of the results shown in Fig. 1, all subsequent calculations use a spherical diffusion geometry to approximate the fragment shape.

Retrieval of diffusion parameters in materials affected by shape anisotropy

The standard Arrhenius relationship used to represent volume diffusion in silicate solids is $D = D_o \exp(-E/RT)$ where D is the diffusivity, D_o is the diffusivity at infinitely high temperature, E is the activation energy, R is the ideal gas constant and T is absolute temperature. We use this relationship to interpret the results from S1 and employ a regression technique that is capable of dealing with step-heating data produced from a material characterized by a distribution of r values (Appendix B in Lovera et al. 1997). The calculated diffusion coefficients define nearly linear arrays with a minor, but resolvable concave-downward curvature evident at high temperature (Fig. 1a). We attribute this effect to glass fragment shape anisotropy. Specifically, low-temperature ^{39}Ar release from near surface regions is sensitive to grain surface irregularities, while gas released from internal regions at high temperatures is not. Hence, we believe that the downward curvature shown in Fig. 1a is produced by a variable, temperature-reliant r that governs Ar transport and increases from smaller to larger values with progressive outgassing.

Correctly estimating activation energy (E) is the most critical step in determining the Ar retention properties from a series of diffusion experiments. In material characterized by a single r, in which Ar transport is described by the Arrhenius relationship, the task is simply accomplished by determining the slope ($-E$/R) defined by an array of diffusion coefficients on a plot of log D/r^2 against inverse T. However, since r in our material is not constant, selection of the data points defining a linear array with a slope parallel to that implied by the apparent E of the sample becomes

problematic. Given the concave-downward curvature exhibited by these data (Fig. 1b), it is clear that the maximum slope defined by a subset of data points will most closely approximate the relevant E of this sample. Balanced against this is the prospect that experimental scatter in a smaller subset of the data could indicate an erroneously high E, or result in a large error associated with E. The goal is to strike a balance between maximizing the size of a data subset that spans a temperature range of interest, while minimizing the associated error in E. However, note that for this sample, the inclusion of additional points would not significantly change the approximated value. This is not necessarily the case for other samples (see discussion below). The best-fit method we employ for sample S1 is one where the number of points used in the regression is increased until the goodness of fit, weighted by the number of points used, reaches a maximum (Fig. 1b inset). The E obtained (26.3 ± 0.3 kcal mol^{-1}) is slightly smaller than the less well-defined value reported in Carroll (1991), but both agree within experimental uncertainty (see Fig. 1a).

Before proceeding to the analysis of our rock-derived glass samples, it is informative to examine the magnitude of the relatively minor increase in the effective r for Ar transport that is implied by the S-glass results. We believe this phenomenon is also related to the physical nature (i.e., shape anisotropy) of S1. The effect can be illustrated graphically by determining the difference between the measured log (D/r^2) values and those implied by the regression array defined in Fig. 1b, and plotting this difference as a function of cumulative ^{39}Ar release (Richter et al. 1991). As indicated in Fig. 1c, effective r increases by a factor of three from that defined by the low-temperature gas release (r_o), which is measurably influenced by the fraction of Ar released from corners and edges around the surface of the grain (i.e., shape anisotropy effects), to that observed just before the sample begins to melt (~1,150 °C). We do not consider the threefold increase in log r/r_o to be unexpected nor significant (with respect to our other glass results) because the increase in effective r is a function of grain properties (size and shape), and the grain r of sample S1 was larger and more irregular than the fragments of other glasses we analyzed. Had fragment S1 been smaller, the effective r (i.e., grain r) would have been closer in length to the r of the small corners and edges of the grain, and the increase in log r/r_o would have been correspondingly small. Also note that this effect influences the fraction of ^{39}Ar used to estimate the diffusion parameters, which for sample S1 is a relatively small fraction of the total gas release (Table 2). One can typically both lessen the impact of shape anisotropy and increase the useful gas fraction for determining diffusion parameters by reducing particle size because doing so results in a larger proportion of the ^{39}Ar occupying near-surface regions. On this basis, we purposely made the fragment sizes for our other glass samples smaller than fragment S1, and tested a range of fragments with different radii (~30–350 μm; Table 2).

Diffusion parameters of pseudotachylyte-derived glasses

We have calculated diffusion parameters for the three pseudotachylyte-derived glass (P-glass) samples, but found it necessary to abandon the automated best-fit method described above and adopt the manual fit procedure discussed below. The P-glass diffusion results are shown in Fig. 2 and listed in Table 2. Recall that four different size fractions were examined for each sample. For most sample fractions, an insignificant portion of the total gas (< 2%) is released at low temperatures (< ~550 °C; see also the Supplementary Electronic Material). Additionally, the majority of the P-glass data

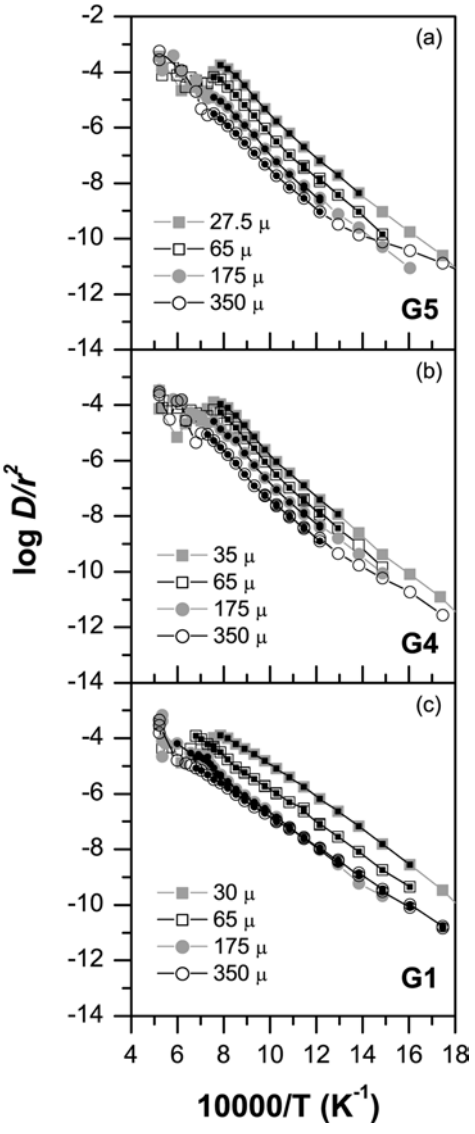

Fig. 2a–c Arrhenius diagrams of Ar diffusion data (unnormalized) from the prepared pseudotachylyte (*P*) glasses; spherical geometry assumed (see text). Data points regressed in the calculation of E shown in *black*. Calculated Arrhenius parameters are given in Table 2. Parameter differences between these glasses are primarily functions of grain shape anisotropy and composition (see Table 1, text discussion)

exhibit a moderate to strong progressive increase in diffusivity between ~650 and ~1,050 °C. The combination of these factors results in concave-upward curvature of the Arrhenius arrays for P4 and P5 glasses (Fig. 2). The automated fitting routine used to determine the Arrhenius parameters for S1 cannot adequately model the concave-upward Arrhenius arrays produced by P4 and P5. Automated fitting was attempted, but the results yielded unrealistically low activation energies that represented less than a few percent of the total ^{39}Ar released. For this reason, fitting was done manually. As discussed above, the goal was to define a reasonably large subset of low-temperature data that produced an E with the smallest error. In general, the initial low-temperature steps are excluded from the fit because they represent $<1\%$ of the cumulative ^{39}Ar yield, and their addition significantly changes E. If initially excluded points could be included into the data subset without affecting E, they were. This manual best-fit approach allows us to account for a large fraction of ^{39}Ar released (Table 2), without significantly increasing the error associated with E.

The following observations can be made from these P-glass diffusion data (Fig. 2, Table 2). First, the Arrhenius parameters for sample P1 are different than P4 and P5. Arrhenius arrays for P1 are near-linear or slightly concave-downward like glass S1, while P4 and P5 arrays are concave-upward. The increase of both E and diffusivity with increasing temperature (i.e., concave-upward curvature) is not without precedent for mafic glasses (cf. Stettler and Bochsler 1979). As this behavior is best illustrated by the AB-glass, it is discussed in the following section. Second, if only P4 and P5 data are considered, intrasample variability of the Arrhenius parameter E, the most critical parameter measured, is minimal and almost all measurements from a given sample agree within uncertainty (Table 2). Third, the average values of E and log D_o for samples P4 and P5 are indistinguishable within error. Fourth, not only is the average value of E for P1 much lower (ca. 10 kcal mol^{-1}) than P4 and P5, there is also no overlap in calculated values of E among the four size fractions (Table 2). We believe the contrasting results between P1 and P4–P5 are in part due to the shape anisotropy effect, which was exaggerated in P1 (especially in the two largest size fractions) because of persistent vesicles. Fifth, for any sample, the average difference (from size fraction to size fraction) in measured D/r^2 at a given temperature is usually reproducible, though about a third less than that anticipated (Fig. 2). For example, for $r = 65$ and $r = 175$ μm fragment sizes, the average difference in measured D/r^2 values is 0.76 ± 0.14, 0.60 ± 0.25, and 0.57 ± 0.20 $\log_{10}$ units (for P1, P4, and P5, respectively) while the calculated difference is 0.86 $\log_{10}$ units. These differences vary proportionally with fragment size (i.e., the largest fragments show the highest discrepancy). Again, we attribute this behavior to shape anisotropy effects. Finally, while the experimentally-determined log D_o and E values reveal intrasample variability, consistent intersample values from P4 and P5 glasses indicate that our step-heating method and data reduction techniques are internally consistent and reproducible.

Diffusion properties of basalt-derived glass and the glass transition effect

The nature and cause(s) of the concave-upward curvature of Arrhenius arrays displayed by the two relatively low-silica P-glasses (P4 and P5; Fig. 2) are further explored with two additional step-heating experiments using two grain-aggregate splits of a basalt-derived glass (AB-glass; Table 1; the Supplementary Electronic Material). Because each of the P-glasses were prepared and analyzed in a consistent manner, and the behavior is consistent from one size fraction of a sample to another, shape anisotropy effects and analytical error can be excluded as causes of the concave-up curvature of glasses P5 and P4. However, among the three P-glasses, composition-dependant effects cannot be ruled out (cf. Table 1, Fig. 2). For this reason, the AB-glass (Table 1) was prepared and analyzed following the procedures used for the P-glasses.

The AB-glass diffusion data (Fig. 3) display a concave-up curvature that is much more pronounced than the more silicic P- and S-glasses. Duplicate isothermal steps were analyzed from the initial heating temperature,

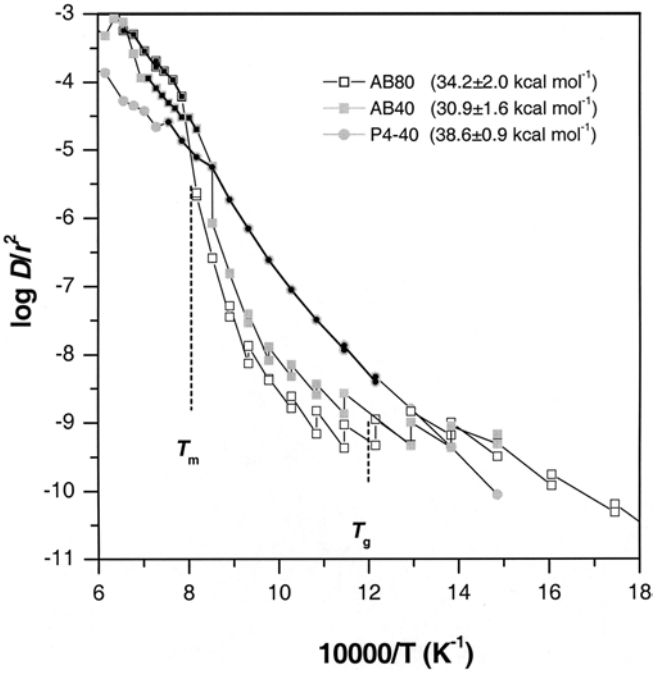

Fig. 3 Arrhenius diagram of Ar diffusion data from prepared, basalt-derived glasses (AB-glass; see Electronic Supplementary Material) and representative pseudotachylyte-derived glass (P4-40; Table 2). Spherical diffusion geometry assumed. *Dashed lines* correspond to the inferred glass transition (T_g) and melting (T_m) temperatures for the AB-glasses. Data points regressed in the calculation of E (*highlighted in black*) and resulting E values are indicated. The strong, non-linear increase in Ar diffusion displayed by AB-glasses is believed to result from changes in the physical properties of these glasses during the transition from solid to supercooled liquid to melt (see discussion in text)

up to ~950 °C. At a given temperature, duplicates generally do not overlap, so determining E is difficult. Below ~900 °C, both AB-glass samples have essentially the same diffusion characteristics (Fig. 3), compared with P-glasses they are generally more retentive, changes in diffusivity appear minimal, and a relatively small fraction of total ^{39}Ar is released (the Supplementary Electronic Material). However, between ~600–650 and 1,000 °C, in striking contrast to the other glasses, the AB-glasses undergo a significant (10^4–10^5) increase in diffusivity with increasing time (t) and T (Fig. 3). For example, over the brief t interval between successive 900 °C isothermal steps, AB40 releases ~15% of the total ^{39}Ar collected. Below 900 °C, the sample had yielded ~3% of the cumulative ^{39}Ar. The initiation of these rapid increases in diffusivity with increasing temperature occurs at ~600 °C (Fig. 3). A second distinct change in the diffusion properties of the basalt glasses occurs at ~1,000 °C. Although much less pronounced, similar inflections are exhibited in the Arrhenius data from P4 and P5 glasses (Fig. 2). Between ~1,000 and ~1,200 °C, the AB-glass Arrhenius data form linear arrays, and over this T interval both AB samples release ~40–70% of their total ^{39}Ar yield. Similar, high-T, linear arrays are observed for some P-glasses.

It has long been recognized from glass diffusion studies (e.g., Stettler and Bochsler 1979) that some glasses can display a positive increase in E and diffusivity during heating, commonly at temperatures well below complete melting (T_m). Although a progressive reduction in effective r during heating (e.g., via grain fracturing) may explain the increase in calculated diffusivity, alternative phenomena are suggested by our diffusion data. By comparing the compositions of the P-, AB-, and S-glasses (Table 1) with their respective diffusion array shapes (i.e., concave-upward versus concave-downward; Figs. 1, 2, and 3), a clear, positive correlation emerges. As the proportion of FeO + MgO + CaO increase relative to SiO_2 + Al_2O3, the upward concavity of the diffusion arrays becomes more pronounced. The concave-upward diffusion curves of glasses P4, P5, and AB typically display two points of inflection (Figs. 2 and 3). In general, data points below the lower inflection and data points above the upper inflection (up to T_m) each form linear trends. Trendline slope-intercept values that describe each of these data sets are dissimilar from one another (i.e., relate different diffusion properties). Between inflection points, the glass is hypothesized to undergo a fundamental physical transformation from glass to supercooled liquid. The onset of this transformation occurs at a specific temperature (T_g; ~2/3 T_m), which is (apparently) composition-dependent (e.g., ~800 °C for albite, ~1,200 °C for silica; Roselieb et al. 1995), and involves a dynamic reorganization (i.e., relaxation) of network structural units as well as the initiation of crystal formation (Hampton and Bailey 1984). The details of this phenomenon and its thermodynamic implications are beyond the scope of this study, but are described by Johnson et al. (1951), Carmichael et al. (p 128; 1974), and Carroll (1991). The goal here is simply to offer explanation for the non-linear Arrhenius behavior displayed by many of our glasses, and explore the implications of this behavior with respect to silicate glasses that may be dated using ^{40}Ar/^{39}Ar step-heating techniques. Based on the AB-glass diffusion results (Fig. 3), the interpreted T_g occurs at the low-T inflection point (i.e., T_g = ~600 °C). Hampton and Bailey (1984) report similar T_g values for their mafic glasses. At the second inflection point (i.e., ~1,000 °C), the transformation from supercooled liquid to a molten state (i.e., T_m) is suggested by the Arrhenius data, and reasonable if our interpreted T_g is correct (i.e., $T_g \approx 2/3\ T_m$).

Determining geologically relevant diffusion parameters from the AB-glass results is problematic. The low-T diffusion results suggest that the AB-glass is very retentive with respect to Ar diffusion (Fig. 3). However, if the same criteria used to determine E for glasses P4 and P5 are applied to the AB-glass data, the low-T results must be excluded from the Arrhenius parameter determination because the isothermal duplicates show no consistent overlap, and these data represent very little of the ^{39}Ar extracted from the sample. The high-T AB-glass data (i.e., ~1,000–1,200 °C), on the other hand, are linear and represent a significant fraction of the total ^{39}Ar released. These data yield an average E of ~36 kcal mol^{-1} (Fig. 3). This result is quite similar to that of the P4 and P5 glasses (Table 2). However, note that the extrapolation of these AB-glass diffusion data, into the range of typical temperatures (i.e., < 350 °C) one might expect during a geologic reheating event, is problematic. Such down-temperature extrapolation of the measured high-T data suggests low-T diffusivities that are more than an order of magnitude lower than the measured low-T data suggest (Fig. 3). In addition, doing so violates a fundamental assumption of the step-heating technique, namely that the material is physically stable over the range of experimental investigation. For these reasons, the Arrhenius parameters of the AB-glasses are deemed too problematic to extract and include with the P- and S-glass results. Fortunately, over the range of T–t conditions for our experiments, Ar diffusion in the P4 and P5 glasses is not as problematic. For most P-glass samples, especially those with small radii, the difference between high- and low-temperature activation energies are minimal (Fig. 2, the Supplementary Electronic Material). While these data further demonstrate that changes in r (i.e., shape anisotropy) influence diffusion non-linearity, the concave-upward form of Arrhenius arrays from the more mafic glasses (P4, P5, AB) indicate that other physical factors (e.g., composition-dependent, temperature-related reorganization of network structural units) can be important.

Effects of physical characteristics upon the Ar retention properties of silicate glasses

Average activation energies (E) reported for silicate glasses range from 22.9–34.5 kcal mol^{-1} (Fig. 4). The mean of these data (~29 kcal mol^{-1}) is lower than the

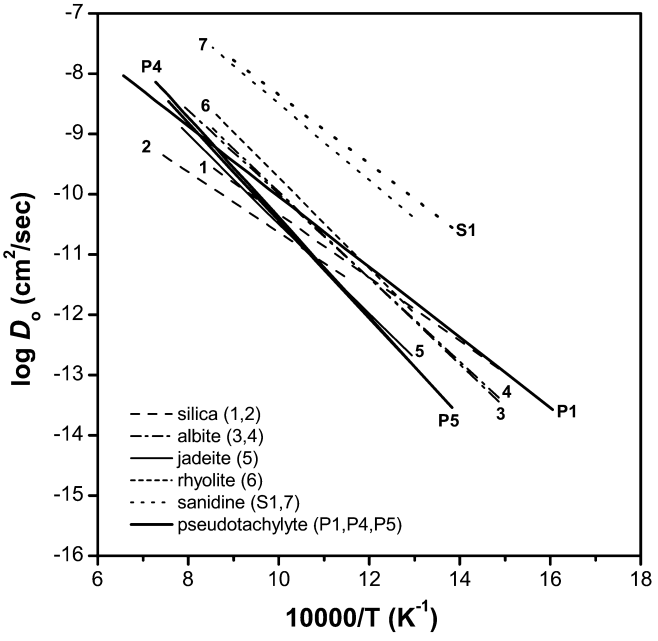

Fig. 4 Summary Arrhenius diagram of average Ar diffusion data from selected silicate glasses. These data suggest that Ar diffusion in P4 and P5 is most like that of rhyolite or albite glass. Ar diffusion in silica-rich P1 is closer to that of fused silica. All data normalized to $r = 1$ cm. Spherical geometry assumed for the S1 and P-glasses; other data use a semi-infinite geometry. *Curve labels* correspond to the following E (in kcal mol^{-1}) and source: P1, P4, P5 (see Table 2; this study); S1 (see Table 2; this study); 1 (24.1 ± 1.3; Carroll and Stolper 1991); 2 (22.9 ± 1.4; Roselieb et al. 1995); 3 (32.8 ± 1.4; Carroll 1991); 4 (31.8 ± 5.7; Roselieb et al. 1995); 5 (33.9 ± 4.1; Roselieb et al. 1995); 6 (34.5 ± 1.5; Carroll 1991); 7 (29.0 ± 3.9; Carroll 1991)

mean of our averaged P-glass data (33.4 ± 0.5 kcal mol^{-1}), due in part to high values calculated for P4 and P5 glasses. The range of reported values is significant because small changes in E can cause large changes in Ar retentivity. The main causes for these variations probably arise from physical factors. Although these factors can be composition-independent (e.g., grain shape anisotropy, differences in experimental technique), the P4–P5 results indicate that other factors are probably not. It has been proposed that Ar retentivity tends to increase as molecular density in the glass increases (Dowty 1980; Carroll and Stolper 1991). Our mafic glass data, which strongly suggest that the abundance of network-modifying Ca, Fe, and Mg is an important control on the diffusion properties of a sample, are consistent with this idea. However, for the moderate to high-silica glasses with low to moderate CaO, FeO, and MgO contents (e.g., most of those shown in Fig. 4), the abundance of SiO_2 and Al_2O_3 must be more important than in the mafic glasses.

It is clear from Fig. 4 that the averaged diffusion properties of different composition glasses (e.g., sanidine, albite, silica, etc.) are distinct. As with other silicate glasses (Carroll 1991; Carroll and Stolper 1991; Roselieb et al. 1992, 1995), SiO_2 and Al_2O_3 are the dominant components and thus a primary control on the molecular density of glasses S1 and P1, and to a lesser extent, glasses P4 and P5. A clear relationship between Ar diffusivity and silica content of silicate glasses shown in Fig. 4 is not observed over the range of temperatures shown. However, based on data shown in Fig. 4, and excluding the end-member pure-silica glasses, the energy of activation does vary proportionally with silica content. If accurate, on the basis of previously published silicate glass diffusion data alone (e.g., Fig. 4), we should be able (to a first-order approximation) to predict the E of our glasses based solely on their compositions. The silica content of glasses P4 and P5 (Table 1) for example, is comparable to albite and rhyolite glass, and indeed the E of all four glasses are identical within error (Fig. 4). Similarly, based on SiO_2 content, the activation energy of glass P1 should be similar to rhyolite or silica glasses (Fig. 4, Table 1). Our data show that the E of P1 is close to that of silica (Fig. 4), but most like that of the sanidine glass (S1), although the diffusivity of P1 is two orders of magnitude lower. We have shown that for similar materials, shape anisotropy effects will likely cause bulk sample D_o estimates to be higher than those yielded by the depth-profiling approach (e.g., Fig. 1a). This effect appears to be on the order of half a $\log_{10}$ unit. If P1 diffusivity is shifted downward by this amount, these data overlap with published silica glass results (Fig. 4). The nearly consistent changes in diffusivity as a function of r (Table 2) leave little doubt that the presence of vesicles (i.e., shape anisotropy) affected P1 diffusion measurements. However, shape anisotropy does not explain the difference between log D_o values of P4 and P5 glasses and those of the albite or rhyolite glasses. The difference is, however, likely caused by the abundance of network-forming Fe, Mg, and Ca cations in P4 and P5. We conclude that the diffusion properties of our glasses are largely governed, directly or indirectly, by material properties such as composition and shape anisotropy.

Simulation of post-slip thermal evolution and implications for dating of silicate glasses

The ability of a simple material such as pure, natural, pseudotachylyte glass to retain radiogenic argon depends upon its diffusion parameters, its effective diffusive length scale, and thermal history it experiences subsequent to formation. As demonstrated above, the diffusion parameters are largely a function of composition. Using the average diffusion parameters determined from our P-glass experiments, bulk closure temperatures were calculated for two, compositional end-member P-glasses (P1 and P4). These data are plotted in Fig. 5 as a function of length scale (i.e., grain r) and cooling rate. Recall that the typical diameter of grains in our starting fault rock is ≤ 100 μm. Over most plausible geologic conditions, bulk closure in a high-silica, low-CaFeMg glass (e.g., P1; Fig. 5a) will occur below ~125–75 °C, while closure in a high-CaFeMg, low-silica glass (e.g.,

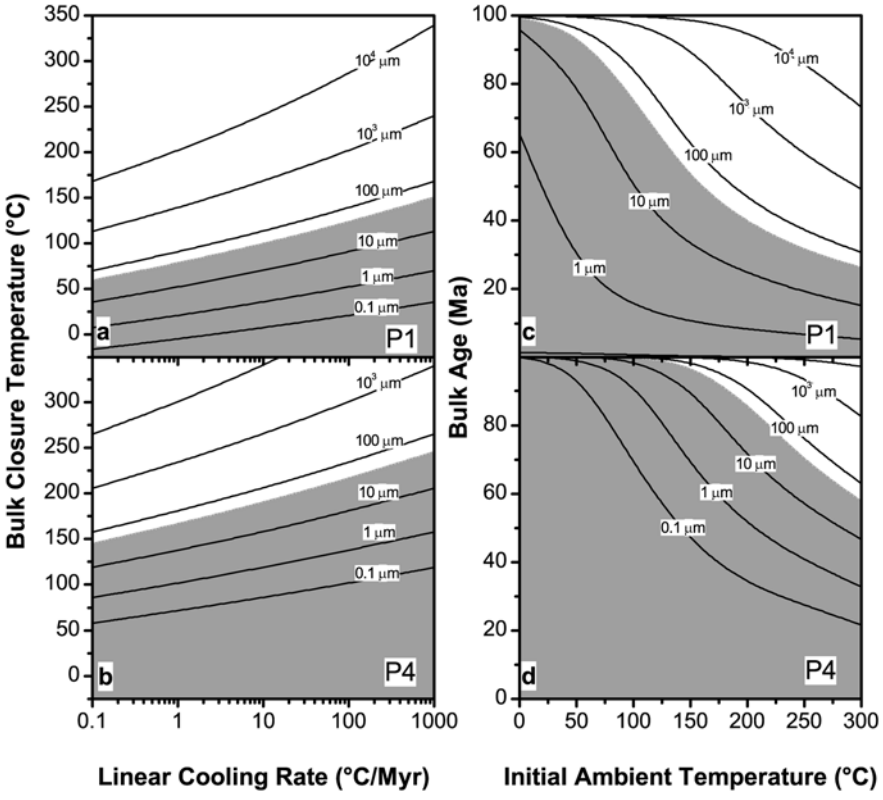

Fig. 5a,b Bulk closure temperature of pseudotachylyte-derived glasses as a function of linear cooling rate and diffusive length scale. Comparison of **a** and **b** show the effect of glass composition. **a** Results using the average high-silica, low-CaFeMg P1 glass data ($D_o = 7.6 \cdot 10^{-5}$ cm^2 s^{-1} and $E = 26.8$ kcal mol^{-1}). **b** Results using the average low-silica, high-CaFeMg P4 glass data ($D_o = 8.8 \cdot 10^{-3}$ cm^2 s^{-1} and $E = 37.8$ kcal mol^{-1}). **c, d** $^{40}Ar/^{39}Ar$ bulk age as a function of diffusive length scale and initial ambient temperature. Models assume slow-cooling of pseudotachylyte glass formed at 100 Ma. Comparison of **c** and **d** show the effect of glass composition; same diffusion properties as in **a** and **b**, respectively. *Shaded regions* highlight the results expected from the average grains (effective $r \leq 50$ μm) in the matrix of typical fault vein pseudotachylyte. Spherical diffusion geometry assumed in all calculations

P4; Fig. 5b) will occur below ~220–165 °C. To illustrate the significance of these retention properties, we calculate bulk closure ages of samples formed at 100 Ma that have undergone simple, linear cooling (Fig. 5). In order to explore a wide range of possible behaviors, we varied the initial ambient temperature (T_{amb}) between 0–300 °C (maximum cooling rate of 3 °C Ma^{-1}), and r from 1 cm to 0.1 μm. While we use a spherical diffusion geometry for these calculations, the use of other geometries would not meaningfully alter conclusions drawn from this exercise. Model results (Fig. 5) show that the region of T_{amb}-r space in which pseudotachylyte glass can quantitatively retain radiogenic Ar (i.e., record the true glass generation age) is relatively restricted, and varies significantly with composition. For example, $r = 1$ cm grains of a comparatively retentive glass (e.g., P4; Fig. 5d) require $T_{amb} < 225$ °C to produce $^{40}Ar/^{39}Ar$ generation ages, while $r < 1$ μm grains experience measurable Ar loss under all conditions (i.e., cooling ages result). In comparison, $r = 1$ cm grains of relatively unretentive glass (e.g., P1; Fig. 5c) require $T_{amb} < 125$ °C to produce $^{40}Ar/^{39}Ar$ generation ages, while $r < 100$ μm grains of the glass experience measurable Ar loss under most conditions.

The implications of these model data with respect to $^{40}Ar/^{39}Ar$ dating of glassy pseudotachylyte are significant. In general, fault vein pseudotachylytes are thought to form during high-speed slip events where fault surface temperatures temporarily reach ≥700 °C (e.g., O'Hara 1992; Lin 1994; Spray 1995), and in tectonically active areas where one would expect background T_{amb} of > 125 °C. The outgassing of Ar at the high temperatures obtained during fault slip, albeit brief, should guarantee that protolith ages will never be obtained. After the initial thermal pulse generated during fault slip (i.e., glass formation), a typical (~1 cm thick) vein would quickly (t~1 day) reach thermal equilibrium with the surrounding host rock at $T = T_{amb}$. Under most reasonable geologic conditions, T_{amb} would probably be far above the average Ar retention temperature of the typical granitoid-derived pseudotachylyte glass. As such, a $^{40}Ar/^{39}Ar$ age from any glassy material within the vein will reflect the time at which the vein/host-rock passed through the temperature required to fully retain Ar in the glass (i.e., cooling age will result). Our calculations indicate that under most such conditions (elevated T_{amb}), one should not expect an average, granitoid-derived, glassy pseudotachylyte to preserve its

formation age unless the analyzed glass grains have a large unfractured diameter. Because pseudotachylyte veins are typically ~1 cm thick or less, and commonly form along long-lived faults or in shear zones where cataclastic reworking and fluid-promoted devitrification are expected, the occurrence of an unfractured, ~1-cm-diameter piece of glass is unlikely. At the scale of average grains that constitute the matrix of the Whipple Mountains pseudotachylytes ($r \leq 50$ μm), the ability of silicate glass to quantitatively retain Ar is much lower than the crystalline, K-bearing, matrix material (e.g., K-feldspar). Assuming that the glass composition reflects the average of our three P-glasses, the unretentive nature will manifest itself in a $^{40}Ar/^{39}Ar$ age obtained from any whole-rock sample (i.e., glass plus crystalline material) or glass separated from crystalline material. For such samples, the $^{40}Ar/^{39}Ar$ ages obtained should be much younger than the time of glass formation (i.e., fault slip). This applies to any other datable glass-bearing geologic material (e.g., tektite, volcanic rock) with compositions similar to our samples. Because small grain sizes are typical of pseudotachylyte matrix, low (post-generation) temperature conditions are required to either obtain generation ages from glassy pseudotachylyte or retrieve approximate generation ages from an otherwise crystalline pseudotachylyte. Thus, pseudotachylyte and tektite glasses that might form at or near the Earth's surface as a result of meteorite impact may yield $^{40}Ar/^{39}Ar$ ages that accurately reflect the age of the impact event; although this remains to be shown for pseudotachylyte glass. Similarly, sufficiently large-diameter glass fragments extracted from volcanic rocks should provide $^{40}Ar/^{39}Ar$ extrusion ages, provided the rocks were never significantly reheated.

Summary and conclusions

Our analytical approach and method of determining Arrhenius parameters differ from most of the previous glass diffusion studies, but are designed to be similar to routine $^{40}Ar/^{39}Ar$ dating studies that use crystalline minerals such as K-feldspar because one of our primary goals is to determine the contribution of glass-derived Ar to $^{40}Ar/^{39}Ar$ pseudotachylyte ages. Experiments performed with sanidine glass (S1) demonstrate that a step-heating approach, based upon progressive degassing of nucleogenic ^{39}Ar produced during neutron irradiation, yields results comparable to those produced by depth-profiling diffusion studies that use K-feldspar glass isothermally heated in an argon reservoir. Minor differences can be attributed to shape anisotropy.

Experiments ($n = 12$) performed with three laboratory-produced, pseudotachylyte-derived silicate glasses (P-glasses) yield average D_o and E values of 4.63×10^{-3} cm^2 s^{-1} and 33.4 kcal mol^{-1}, respectively. These values generally agree well with previously reported silicate glass Ar diffusion results ($E = 22.9$–34.5 kcal mol^{-1}). A step-heated, high-silica, pseudotachylyte-derived glass sample yields the lowest activation energy and has Arrhenius properties that are consistent with previous results from silica glass depth-profiling experiments. The Ar diffusion properties of the other two pseudotachylyte-derived glasses resemble those obtained previously from rhyolite and albite glass depth-profiling.

On an Arrhenius diagram, nearly all diffusion data from the P-glasses plot as non-linear curves. The high-silica sample (P1) data arrays are all sub-linear, or show a gentle concave-down curvature. We attribute this non-linearity to grain shape anisotropy (i.e., non-ideal surface geometry) effects that resulted from crushing and vesiculation during the glass preparation stage. Conversely, the relatively low-silica P-glasses (P4 and P5) display gentle to moderate concave-up non-linearity. We believe that this may be primarily caused by structural changes involving network-modifying cations (i.e., Ca, Fe, and Mg), although a grain fracturing effect cannot be excluded.

To investigate the possible connection between glass compositions and direction of data curvature on an Arrhenius plot, a silica-poor, CaFeMg-rich, basalt-derived glass (AB-glass) was also step-heated. On an Arrhenius diagram AB-glass diffusion data reveal a strong concave-upward curvature (i.e., increase in E and D) between T of ~600 and 1,000 °C. The interpreted cause of this behavior is also attributed to the abundance of Fe, Mg, and Ca, and the reorganization of network structural units, coupled with mineral crystallization (and eventual resorption), which occurs prior to complete fusion. These processes facilitate rapid increases in the flux of Ar from these grains with increasing T and t. At $T > 1{,}000$ °C, the AB-glass diffusion data are linear and provide an average E of ~32 kcal mol^{-1}, which is consistent with the average P-glass results. However, these high-T AB-glass Arrhenius results are not representative of the low-T (< 600 °C) data, and we argue that such down-temperature extrapolation should be avoided for FeMgCa-rich, low-silica glasses. In such glasses, estimates of noble gas diffusion rates at low temperatures (i.e., geologic conditions) that are based on extrapolations from existing laboratory time-scale, high-T, diffusion experiments should be viewed with caution until independently verified.

Using the P-glass results, simple simulations of a thermal history evolution in which initial ambient temperature and diffusion length scale are varied, and temperature falls linearly to surface conditions over a 100-Ma interval, indicate that the conditions for quantitative retention of radiogenic Ar are quite restricted and vary with glass composition. In general, these results indicate that millimeter- to centimeter-scale fragments of average granitoid-derived pseudotachylyte glass from low ambient temperature environments (e.g., $T_{amb} < 65$–175 °C) are capable of preserving formation ages. Sub-millimeter to micron-scale glass bodies prevalent in some pseudotachylytes that are formed in all but the shallowest crustal settings will only record cooling ages.

Still, assuming a bulk composition similar to the average of our P-glasses, reasonably accurate $^{40}Ar/^{39}Ar$ pseudotachylyte generation ages should be expected from the glassy portions of pseudotachylytes that form in the upper ~2 km of crust (assuming an average geothermal gradient of 25 °C km^{-1}), from pseudotachylyte and tektite glasses that form as a result of meteorite impact and rapidly cool at the Earth's surface, and from volcanic glasses that have not experienced significant post-eruption reheating (e.g., via burial). The results of this diffusion study indicate that additional experimental and physical constraints should be determined for the non-glassy components of typical pseudotachylyte matrix before $^{40}Ar/^{39}Ar$ pseudotachylyte ages can be unambiguously interpreted as either generation or cooling ages.

Acknowledgements The authors wish to thank Marty Grove for his assistance with the experiments and early manuscript versions, and Pete Burnard, Steve Reddy, and an anonymous reviewer for their critiques. Craig Manning and Frank Kyte provided aid with and use of lab facilities. This project was supported by National Science Foundation grants EAR9219472 (Axen) and EAR9814779 (Axen). Lovera was also supported by a grant from the Department of Energy (DE-FG-03-89ER14049, Harrison).

References

Anderson JL, Cullers RL (1990) Middle to upper crustal plutonic construction of a magmatic arc; an example from the Whipple Mountains metamorphic core complex. In: Anderson JL (ed) Nature and origin of Cordilleran magmatism, Mem 174. Geological Society of America, Boulder, pp 47–69

Carmichael I, Turner FJ, Verhoogen J (1974) Igneous petrology. McGraw-Hill, San Francisco

Carroll MR (1990) Simultaneous determination of inert gas solubility and diffusivity in glasses at elevated temperatures and pressures. J Non-Cryst Solids 124(2–3):181–185

Carroll MR (1991) Diffusion of argon in rhyolite, orthoclase, and albite composition glasses. Earth Planet Sci Lett 103(1–4):156–168

Carroll MR, Stolper EM (1991) Argon solubility and diffusion in silica glass: Implications for the solution behavior of molecular gases. Geochim Cosmochim Acta 55(1):211–225

Davis GA, Anderson JL (1991) Low-angle normal faulting and rapid uplift of mid-crustal rocks in the Whipple Mountains metamorphic core complex, southeastern California; discussion and field guide. In: Walawender M, Hanan BB (eds) Geological excursions in southern California and Mexico. Geological Society of America, Boulder, pp 417–446

Dowty E (1980) Crystal-chemical factors affecting the mobility of ions in minerals. Am Mineral 65(1–2):174–182

Hampton CM, Bailey DK (1984) Gas extraction experiments on volcanic glasses. J Non-Cryst Solids 67:147–168

Hazelton G, Axen GJ, Grove M (1998a) Pseudotachylyte formation during seismogenic low-angle normal faulting, Whipple detachment fault (WDF), SE California. Abs w/ Prog GSA 30:19

Hazelton G, Grove M, Axen GJ (1998b) Kinetics of Ar in pseudotachylyte from the Whipple Mountains, CA. EOS 79(46):F875

Hazelton G, Grove M, Axen GJ (1999) Argon diffusion in pseudotachylyte and glass: Implications for the development of a pseudotachylyte chronometer. EOS 80(46):F1026

Johnson JR, Bristow RH, Blau HH (1951) Diffusion of ions in some simple glasses. J Am Ceram Soc 34(6):165–172

Karson JA, Brooks CK, Storey M, Pringle MS (1998) Tertiary faulting and pseudotachylytes in the East Greenland volcanic rifted margin; seismogenic faulting during magmatic construction. Geology 26(1):39–42

Kelley SP, Reddy SM, Maddock R (1994) Laser-probe $^{40}Ar/^{39}Ar$ investigation of a pseudotachylyte and its host rock from the Outer Isles Thrust, Scotland. Geology 22(5):443–446

Lin A (1994) Glassy pseudotachylyte veins from the Fuyun fault zone, northwest China. J Struct Geol 16(1):71–83

Lovera OM, Grove M, Harrison TM, Mahon KI (1997) Systematic analysis of K-feldspar $^{40}Ar/^{39}Ar$ step heating results; I, significance of activation energy determinations. Geochim Cosmochim Acta 61(15):3171–3192

Lovera OM, Grove M, Harrison TM (2002) Systematic analysis of K-feldspar $^{40}Ar/^{39}Ar$ step heating results; II, relevance of laboratory argon diffusion properties to nature. Geochim Cosmochim Acta 66(7):1237–1255

Magloughlin JF, Spray JG (1992) Frictional melting processes and products in geological materials - introduction and discussion. Tectonophysics 204(3–4):197–206

McDougall I, Harrison TM (1999) Geochronology and thermochronology by the $^{40}Ar/^{39}Ar$ method. Oxford University Press, New York

O'Hara K (1992) Major- and trace-element constraints on the petrogenesis of a fault-related pseudotachylyte, western Blue Ridge Province, North Carolina. Tectonophysics 204(3–4):279–288

Parsons I, Brown WL, Smith JV (1999) $^{40}Ar/^{39}Ar$ thermochronology using alkali feldspars; real thermal history or mathematical mirage of microtexture? Contrib Mineral Petrol 136(1–2):92–110

Ray SK (1999) Transformation of cataclastically deformed rocks to pseudotachylyte by pervasion of frictional melt; inferences from clast-size analysis. Tectonophysics 301(3–4):283–304

Reimold WU (1995) pseudotachylyte in impact structures; generation by friction melting and shock brecciation? A review and discussion. Earth-Sci Rev 39(3–4):247–265

Reimold WU, Jessberger EK, Stephan T (1990) $^{40}Ar/^{39}Ar$ dating of pseudotachylyte from the Vredefort Dome, South Africa; a progress report. Tectonophysics 171(1–4):139–152

Richter FM, Lovera OM, Harrison TM, Copeland P (1991) Tibetan tectonics from $^{40}Ar/^{39}Ar$ analysis of a single K-feldspar sample. Earth Planet Sci Lett 105(1–3):266–278

Roselieb K, Rammensee W, Buettner H, Rosenhauer M (1992) Solubility and diffusion of noble gases in vitreous albite. Chem Geol 96(3–4):241–66

Roselieb K, Rammensee W, Buttner H, Rosenhauer M (1995) Diffusion of noble gases in melts of the system SiO_2–$NaAlSi_2O6$. Chem Geol 120(1–2):1–13

Scott JS, Drever HI (1953) Frictional fusion along a Himalayan thrust. Trans R Soc Edinb Biol 65(part 2):121–140

Shand SJ (1916) The pseudotachylyte of Parijs (Orange Free State). Q J Geol Soc Lond 72:198–221

Sibson RH (1975) Generation of pseudotachylyte by ancient seismic faulting. Geophys J Roy Astrol Soc 43(3):775–794

Sibson RH (1977) Fault rocks and fault mechanisms. J Geol Soc Lond 133(part 3):191–213

Sinha-Roy S (1981) Pseudotachylyte from a thrust zone in mylonitic gneisses of major Bergen Arc, South West Norway. Neues Jahrb Mineral 141(2):150–160

Spray JG (1995) Pseudotachylyte controversy; fact or friction? Geology 23(12):1119–1122

Spray JG, Kelley SP, Reimold WU (1995) Laser probe $^{40}Ar/^{39}Ar$ dating of coesite- and stishovite-bearing pseudotachylytes and the age of the Vredefort impact event. Meteoritics 30(3):335–343

Stettler A, Bochsler P (1979) He, Ne and Ar composition in a neutron activated sea-floor basalt glass. Geochim Cosmochim Acta 43(1):157–170

Thompson LM, Spray JG, Kelley SP (1998) Laser probe $^{40}Ar/^{39}Ar$ dating of pseudotachylyte from the Sudbury Structure; evidence for postimpact thermal overprinting in the North Range. Meteorit Planet Sci 33(6):1259–1269

Trieloff M, Reimold W, Kunz J, Boer R, Jessberger E (1994) $^{40}Ar/^{39}Ar$ thermochronology of pseudotachylyte at the Ventersdorp Contact Reef, Witwatersrand basin. S Afr J Geol 97(3):365–382

Tsutsumi A (1999) Size distribution of clasts in experimentally produced pseudotachylytes. J Struct Geol 21(3):305–312

Wenk HR (1978) Are pseudotachylytes products of fracture or fusion? Geology 6(8):507–511

Wenk HR, Johnson LR, Ratschbacher L (2000) Pzseudotachylytes in the eastern Peninsular Ranges of California. Tectonophysics 321(2):253–277

White BS, Brearley M, Montana A (1989) Solubility of argon in silicate liquids at high pressures. Am Mineral 74(5–6):513–529

Yoder HS, Tilley CE (1962) Origin of basalt magmas; an experimental study of natural and synthetic rock systems. J Petrol 3(part 3):342–532